



# Dopamine-derived N-doped carbon-encapsulated MoS<sub>2</sub> microspheres as a high-performance anode for sodium-ion batteries

Hua Qiu<sup>1</sup> · Hongyu Zheng<sup>1</sup> · Yuhong Jin<sup>2,3</sup> · Miao Jia<sup>1</sup> · Qiong Yuan<sup>1</sup> · Chenchen Zhao<sup>2,3</sup> · Mengqiu Jia<sup>1</sup>

Received: 17 May 2020 / Revised: 11 July 2020 / Accepted: 5 August 2020 / Published online: 12 August 2020  
© Springer-Verlag GmbH Germany, part of Springer Nature 2020

## Abstract

Two-dimensional lamellar MoS<sub>2</sub> has been widely studied as an anode material for sodium-ion batteries. However, MoS<sub>2</sub> exhibits low electrical conductivity and large volume change during the electrochemical charge-discharge process, resulting in poor electrochemical performance. In this work, the dopamine-derived N-doped carbon-encapsulated MoS<sub>2</sub> microsphere (MoS<sub>2</sub>@NC) composite material was synthesized and employed as anode material for sodium-ion batteries (SIBs). As-prepared MoS<sub>2</sub>@NC composites exhibited an excellent cycle performance with high specific capacity of 480 mAh g<sup>-1</sup> at a current density of 100 mA g<sup>-1</sup> after 100 cycles and outstanding rate capability (the capacities of 484, 456, 425, 408, and 393 mAh g<sup>-1</sup> at 0.1, 0.2, 0.5, 1, and 2 A g<sup>-1</sup>, respectively). The good electrochemical sodium storage performance for MoS<sub>2</sub>@NC is probably attributed to N-doped carbon layer on the surface of MoS<sub>2</sub>, which can effectively suppress the volume expansion of MoS<sub>2</sub>, increase the electric conductivity and limit contact with electrolyte.

**Keywords** MoS<sub>2</sub> · N-doped carbon · Dopamine · Anode materials · Sodium-ion batteries

## Introduction

In recent years, due to the shortage of lithium resources, sodium-ion batteries (SIBs) arouse wide concern. Compared with lithium, sodium has many advantages such as abundant natural resources and low cost [1, 2]. The physical and chemical properties of sodium are similar to lithium. Therefore, it is considered that SIBs are the most likely to replace lithium-ion batteries (LIBs) as a new type of secondary batteries. However, SIBs have some inherent defects. For example, first, sodium atomic mass is also larger than the lithium, which will lead to a lower theoretical capacity of sodium-ion batteries [3,

4]. Second, the atomic radius of sodium ions is 0.106 nm which is larger than that of lithium ions by 0.076 nm. It will increase the diffusion barrier during the charging and discharging [5–8]. Under this circumstance, it is urgent to design efficient anode materials for SIBs.

In recent years, metal sulfides have been researched as anode materials for SIBs due to their excellent electrochemical performance in reacting with sodium [9–11]. Among them, MoS<sub>2</sub> has drawn scientists' attention [12, 13]. MoS<sub>2</sub> has a sandwich structure that a single layer of MoS<sub>2</sub> has sulfur atoms on the upper and lower layers and a molybdenum atom on the middle layer [14]. This type of structure contains strong covalent bonds between layers and weak van der Waals forces between layers [15–18]. Multilayer MoS<sub>2</sub> is composed of several single-layer MoS<sub>2</sub>, with a layer spacing of approximately 0.62 nm. The spacing between the sheets can ensure the free movement of sodium ions, which leads to good sodium storage performance [19, 20]. However, tremendous volume change and the low electronic conductivity during cycling limit the practical application of MoS<sub>2</sub> as an anode material of SIBs [21–23]. Recently, researchers have been done a lot of work to solve this problem. Cheng et al. [24] used the electrospinning method to embed a single-layer MoS<sub>2</sub> in amorphous carbon nanofibers. As-obtained hierarchical MoS<sub>2</sub>/carbon nanofibers structure used as anode material in SIBs

✉ Yuhong Jin  
jinyh@bjut.edu.cn

✉ Mengqiu Jia  
jiamq@mail.buct.edu.cn

<sup>1</sup> Beijing Key Laboratory of Electrochemical Process and Technology for Materials, Beijing University of Chemical Technology, Beijing 100029, China

<sup>2</sup> The College of Materials Science and Engineering, Beijing University of Technology, Beijing 100124, China

<sup>3</sup> Beijing Guyue New Materials Research Institute, Beijing University of Technology, Beijing 100124, China

delivered a stable capacity of 485 mAh g<sup>-1</sup> at 100 mA g<sup>-1</sup> for 100 cycles. Lin et al. [25] used popcorn as carbon source to build MoS<sub>2</sub>/popcorn-derived carbon composites, which facilitated the electronic transfer and ion diffusion. It demonstrated a reversible capacity of 406.9 mAh g<sup>-1</sup> at 200 mA g<sup>-1</sup> after 340 cycles. Wang et al. [26] developed a heterogeneous system structure composed of MoS<sub>2</sub>-coupled carbon nanosheets wrapped nanowires in sodium titanate. The unique structure displayed excellent performance with a reversible capacity of 425.5 mAh g<sup>-1</sup> at 200 mA g<sup>-1</sup>. Hu et al. [27] utilized salt template to disperse MoS<sub>2</sub> into 3D porous carbon. The carbon framework inhibited the volume expansion during charging/discharging. This MoS<sub>2</sub>/C composite showed a capacity of 372 mAh g<sup>-1</sup> at 0.5 A g<sup>-1</sup> for 200 cycles as an anode material for SIBs. However, the existing methods needed special equipment and had complicated preparation steps. Most importantly, in our group, we have studied the effect of dopamine-derived N-doped carbon coating on the electrochemical Na storage performance of active anode materials (Sn<sub>4</sub>P<sub>3</sub> [28] and NiCoSe<sub>2</sub> [29]). We found that dopamine-derived N-doped carbon coating was a promising and effective method to enhance the anode materials with the conversion reaction mechanism.

Herein, we used a convenient hydrothermal method to prepare flower-like MoS<sub>2</sub>. Then, the dopamine-derived N-doped carbon-encapsulated MoS<sub>2</sub> microspheres (MoS<sub>2</sub>@NC) composite material was prepared by in situ self-polymerization of dopamine on the surface of the flower-like MoS<sub>2</sub> microspheres, followed by carbonization. When employed as anode material in SIBs, MoS<sub>2</sub>@NC anode showed excellent rate performance and cycle performance (a high specific capacity of 480 mAh g<sup>-1</sup> at 100 mA g<sup>-1</sup> after 100 cycles). The results demonstrate that the composites can be superior SIBs anode material.

## Experimental

### Synthesis of pure flower-like MoS<sub>2</sub> materials

All chemical reagents used were purchased from Sinopharm Chemical Reagent Co., Ltd., and used without further purification. Pure flower-like MoS<sub>2</sub> materials were prepared by a simple hydrothermal method. Typically, 0.5 g of sodium molybdate and 1 g of thiourea were mixed in 80-mL deionized water and stirred well. Subsequently, the prepared solution was transferred to a 100-mL Teflon-lined autoclave to heat at 180 °C for 24 h. After cooling down to room temperature, the solution was centrifuged to collect the product and washed with deionized water and ethanol multiple times. Finally, the pure MoS<sub>2</sub> obtained was put into an oven and dried overnight at 60 °C.

### Synthesis of MoS<sub>2</sub>@NC nanocomposites

By stirring at room temperature for 3 h, dissolve 200 mg of the prepared flower-like MoS<sub>2</sub> and 200 mg of dopamine hydrochloride in 200 mL of Tris-buffer solution (10 mM). Then, the product was collected by centrifugation and washed multiple times with deionized water and ethanol. Subsequently, it dried at 80 °C overnight. Then, the dried material was sintered at 600 °C for 2 h under N<sub>2</sub> atmosphere (heating rate 5 °C min<sup>-1</sup>) to obtain MoS<sub>2</sub>@NC powder.

### Characterization

We used an X-ray powder diffraction (XRD) instrument which is Rigaku D/max-2500 with Cu K radiation (= 1.54056 Å) to characterize the sample's crystal structure and used Raman JY-HR800 to test Raman analysis. An X-ray photoelectron spectroscopy (XPS) instrument (ESCALAB 250) mainly performs qualitative and quantitative analysis of elements, solid surface analysis, and compound structure analysis by determining the binding energy of electrons. The thermal gravimetric analysis (TGA) was mainly used to determine the content of each component in the composite material. We used a scanning electron microscope (FESEM, JSM-7001F) and a transmission electron microscope (TEM, Hitachi 800) to measure the morphology and structure of MoS<sub>2</sub> and MoS<sub>2</sub>@NC composite materials.

### Electrode preparation and electrochemical measurements

The active material was mixed with the conductive agent (Super P) and the binder (acetylene black) according to the mass ratio of 7: 2: 1, and then appropriate amount of water was added as a solvent, and the slurry with moderate viscosity and uniformity was obtained by grinding. The prepared mixed slurry was poured on the copper foil that was dried and cooled in advance, the slurry was applied to the copper foil evenly according to the required thickness, and then it was transferred to a vacuum drying oven at 120 °C for 10 h under vacuum drying. The prepared pole piece was used as the working electrode. The metal potassium piece was used as the counter electrode. The Whatman GF/D type cellulose membrane was used as the separator (pre-cut into a 16-mm-diameter disc) with the electrolyte (v/v = 1: 1) with 5.0% FEC. The CS350 electrochemical workstation was used for CV testing (voltage scanning range is 0.01–3.0 V, and the scanning rate is 0.1 mV s<sup>-1</sup>). We used electrochemical workstation (CS310) to measure electrochemical impedance spectra (EIS, 5 mV, 100 kHz–0.01 Hz). The experiment used the Neware (CT-3008W-5V10mA-A4) BTS series high-precision battery test system for electrochemical performance testing.

## Results and discussion

We use XRD analyses to characterize the crystalline of the as-prepared pure MoS<sub>2</sub> and MoS<sub>2</sub>@NC composites. As shown in Fig. 1, in the XRD pattern of the as-prepared MoS<sub>2</sub> and MoS<sub>2</sub>@NC composites, the diffraction peaks at 13.5°, 32.4°, 35.8°, 43°, and 57° can correspond to the (002), (100), (103), (105) and (110) planes, respectively. All these diffraction peaks can be assigned to a hexagonal MoS<sub>2</sub> crystal (JCPDS No. 37-1492) [30, 31].

Figure 2 shows the Raman spectra of MoS<sub>2</sub>@NC composites. It can be observed that the spectra of MoS<sub>2</sub>@NC composites contain the characteristic peaks of carbon materials (~1350 cm<sup>-1</sup> disorder D peak, ~1590 cm<sup>-1</sup> graphitized G peak). The intensity ratio of *I*<sub>D</sub> and *I*<sub>G</sub> is often used to characterize the degree of order of the crystal structure of carbon materials. The *I*<sub>D</sub>/*I*<sub>G</sub> of MoS<sub>2</sub>@NC is 1.08, which is significantly larger than that of graphene oxide (~0.9). The generation of CO<sub>2</sub> during heat treatment will cause more carbon vacancies and significantly increase the disorder of the composite. These defects also provide more active sites for the molybdenum sulfide. In addition, MoS<sub>2</sub>@NC composites have characteristic MoS<sub>2</sub> peaks located at 331 and 371 cm<sup>-1</sup>, which represent two forms of E<sub>2g</sub><sup>1</sup> and A<sub>g</sub><sup>1</sup> vibration for hexagonal MoS<sub>2</sub>, respectively. Among them, the vibration form of E<sub>2g</sub><sup>1</sup> originates from the vibration of two opposite S atoms with respect to the molybdenum atom, while the vibration form of A<sub>g</sub><sup>1</sup> and only the S-atom along the c-axis is the only form of vibration [30, 31]. XRD and Raman results show that molybdenum sulfide and its composites are successfully synthesized.

The elemental composition of the prepared sample is tested by XPS. Figure 3 shows the main elements of MoS<sub>2</sub>@NC based on XPS core-level spectra. Figure 3 a is an S 2p energy spectrum. The two peaks of sulfur at 161.7 eV and 162.9 eV

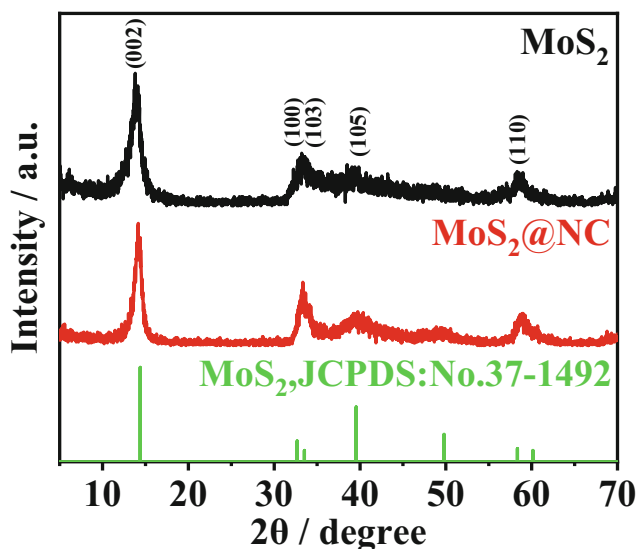


Fig. 1 XRD patterns of pure MoS<sub>2</sub> and MoS<sub>2</sub>@NC composites

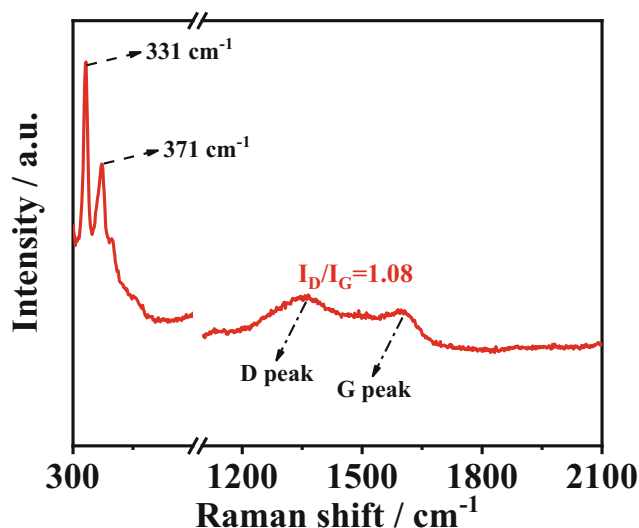


Fig. 2 Raman spectra of MoS<sub>2</sub>@NC composites

represent the binding energy of S elements 2p<sub>2/3</sub> and 2p<sub>1/2</sub>, respectively, indicating that sulfur exists in the composite as S<sup>2-</sup>. Meanwhile, the S 2p spectrum contains a S<sup>6+</sup> peak at 168.7 eV. Compared with that of S<sup>2-</sup> 2p, the proportion of S<sup>6+</sup> 2p peaks is very small, which may be due to the oxidation of S<sup>2-</sup> in the atmosphere [32]. Figure 3 b shows that there are two sharp peaks at 228.9 eV and 232.1 eV, corresponding to the 3d<sub>5/2</sub> and 3d<sub>3/2</sub> orbital electron energy of Mo element, respectively, which proves the existence of tetravalent molybdenum ions in MoS<sub>2</sub>. From Fig. 3c, C-C, C-N, and C-C=O are located at 284.7, 286, and 289 eV, respectively. As shown in Fig. 3c, it shows that the N element is confirmed to have doped into the carbon matrix due to the presence of C-N. Meanwhile, as shown in Fig. 3 d, the N1s spectrum is fitted with three peaks: pyridine nitrogen (N1), pyrrole nitrogen (N2), and graphitized nitrogen (N3), with corresponding energies of 398.3, 400.2, and 401.4 eV, respectively. Additionally, it can be seen from Fig. 3a that the composite material is mainly composed of four elements: C, O, Mo, and S. Moreover, further analysis shows that the atomic ratio of the two elements of molybdenum and sulfur is about 2:1, which can also explain the existence of molybdenum sulfide. These results further confirm the composition of the nitrogen-doped MoS<sub>2</sub>@NC composite.

In order to determine the relative content of molybdenum sulfide and carbon components in MoS<sub>2</sub>@NC composites, thermal weight loss analysis (TGA) tests were performed in an air atmosphere. It can be seen from Fig. 4 that the mass loss of the composite material mainly has three parts. The mass loss at about 400 °C is caused by the conversion of MoS<sub>2</sub> to MoO<sub>3</sub> [32]. The mass loss at about 450–550 °C is caused by the reaction of carbon. The mass loss above 700 °C is mainly caused by the sublimation of molybdenum trioxide. It can be seen from the test results that the mass fraction of carbon in MoS<sub>2</sub>@NC composites is 8.63%.

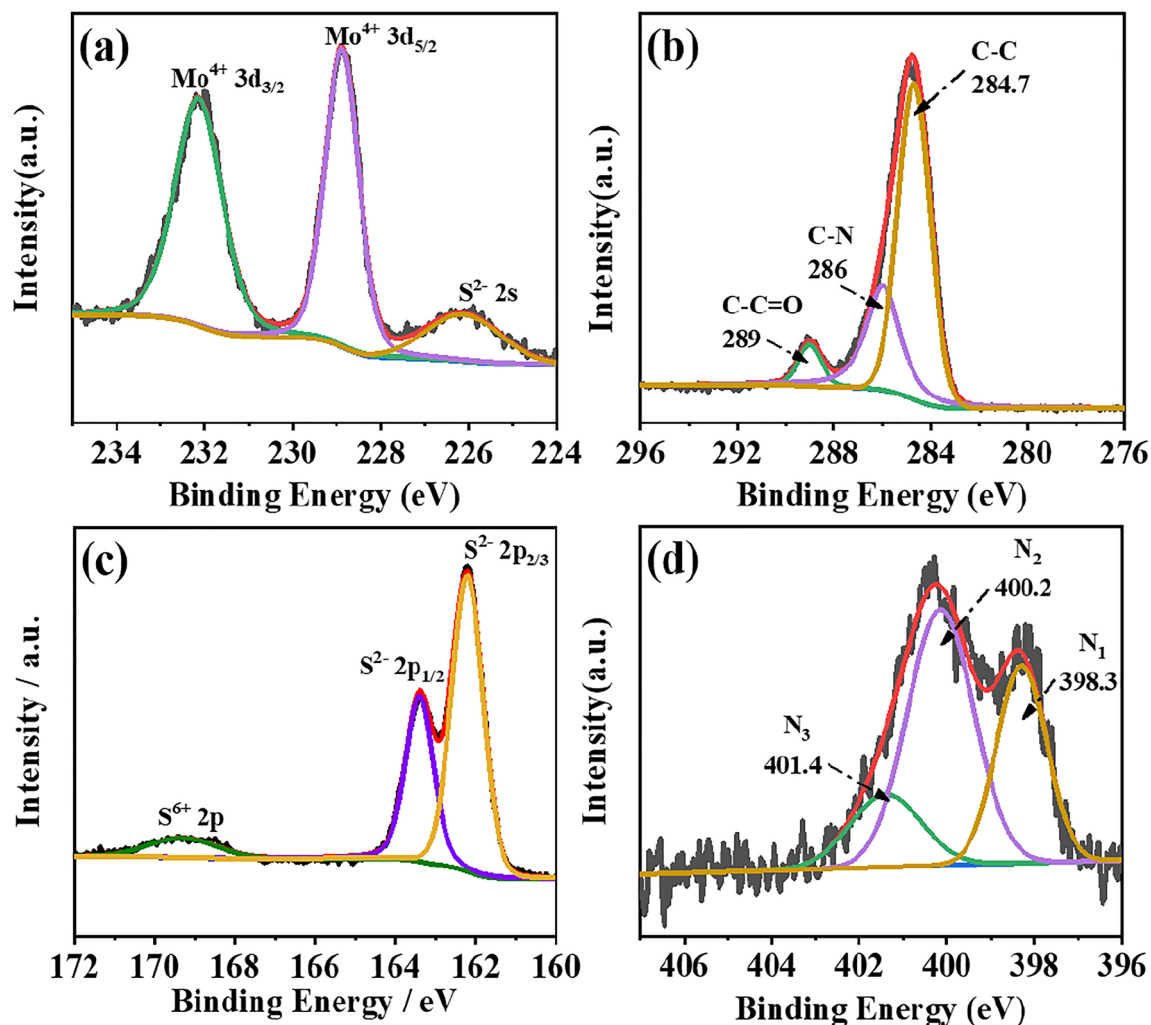


Fig. 3 XPS spectra of **a** Mo3d, **b** C1s, **c** S2p, and **d** N1s regions of MoS<sub>2</sub>@NC composites

The morphology, microstructure, and formation process of flower-like MoS<sub>2</sub> and MoS<sub>2</sub>@NC composites are characterized by FESEM and TEM. From Fig. 5a, b, it can be seen that MoS<sub>2</sub> nanoparticles have a clear flower-like structure. When

dopamine-derived carbon is coated on flower-like MoS<sub>2</sub> nanoparticles, it can be seen from Fig. 5c, d that MoS<sub>2</sub> nanoparticles can still maintain a flower-like structure. From Fig. 5d, e, the surface of flower-like MoS<sub>2</sub> nanoparticles is covered with carbon coating. This shows that the precursor structure can be maintained well when preparing MoS<sub>2</sub>@NC composites.

As shown in Fig. 6a, during the first cathode scan, the reduction peak at 0.8 V corresponds to the interlayer formation of the sodium ion to the molybdenum sulfide layer and the SEI film. The reduction peak at 0.6 V corresponds to the conversion of sulfide to Mo. In the first anode process, the oxidation peak at 1.7 V corresponds to the conversion of Mo to molybdenum sulfide. In the next few cycles, the electrode material showed good cycle stability, and the reaction formula:  $\text{MoS}_2 + 4\text{Na}^+ + 4\text{e}^- \rightarrow \text{Mo} + 2\text{Na}_2\text{S}$  [33–35]. Pure MoS<sub>2</sub> and MoS<sub>2</sub>@NC have the same sodium storage mechanism. Figure 6 b shows Charge-discharge curves at 0.1 A g<sup>-1</sup> of the pure MoS<sub>2</sub> for SIBs. MoS<sub>2</sub>@NC electrode provides initial discharge and charge capacities of 682 and 550 mAh g<sup>-1</sup> at

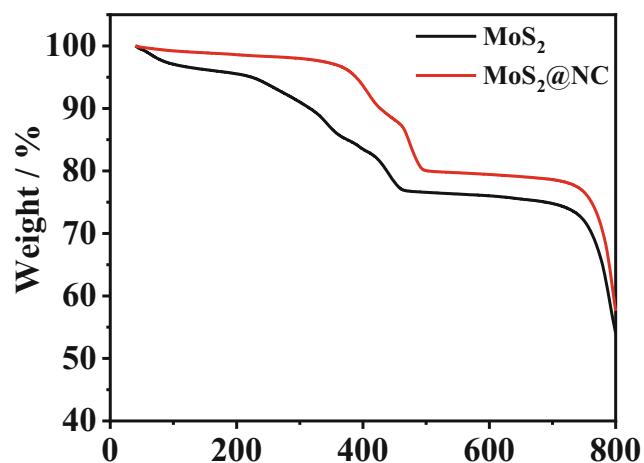
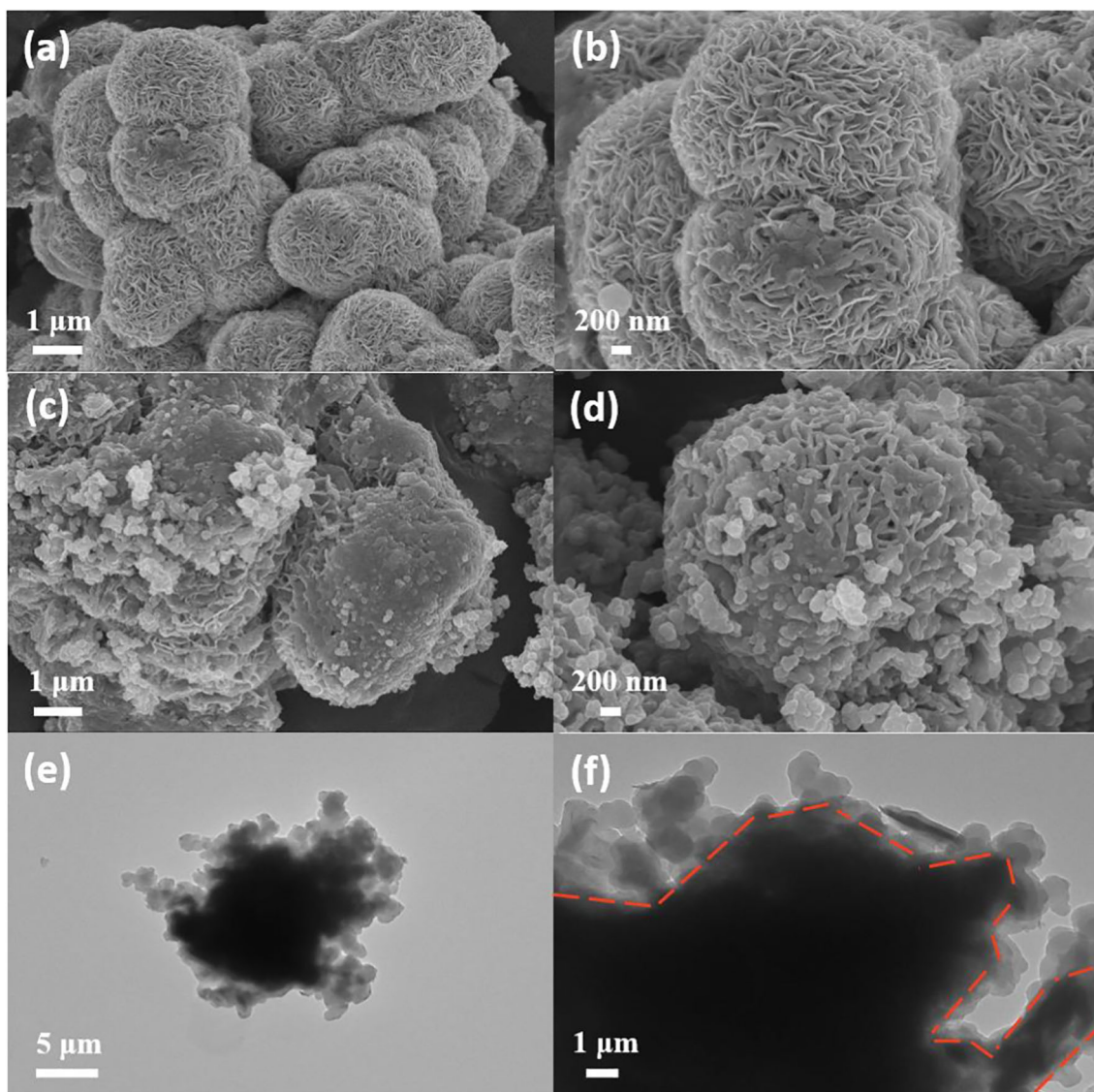


Fig. 4 TGA curves of MoS<sub>2</sub> nanoflakes and MoS<sub>2</sub>@NC composites



**Fig. 5** SEM images of **a, b** pure MoS<sub>2</sub> and **c, d** MoS<sub>2</sub>@NC composites; **e, f** TEM images of MoS<sub>2</sub>@NC composites

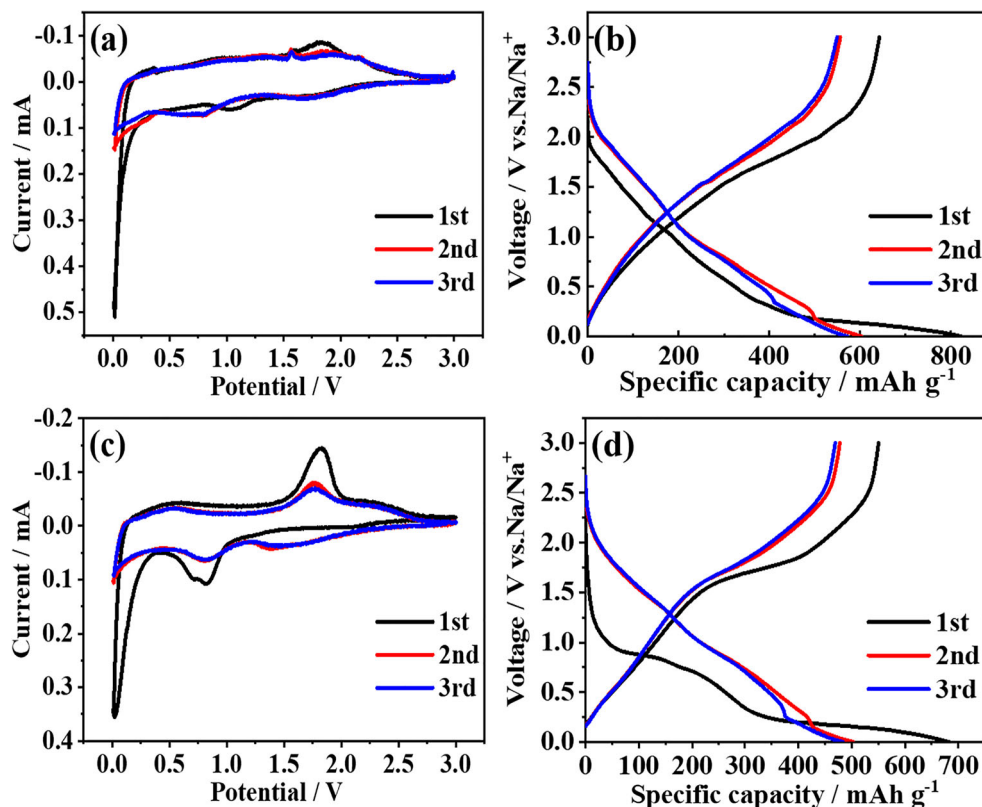
0.1 A g<sup>-1</sup>, respectively, showing initial coulombic efficiency (ICE) of 80.6%. Meanwhile, the ICE of MoS<sub>2</sub> is 78.2%. SEI is formed on the surface of the electrode material during the first discharge, which results in partial capacity loss.

Figure 7 shows the rate performance of MoS<sub>2</sub>@NC and pure MoS<sub>2</sub> as anodes for SIBs at the current density of 0.1, 0.2, 0.5, 1, 2, and 0.1 A g<sup>-1</sup>. It is evident that MoS<sub>2</sub>@NC composites have great rate performance, while pure MoS<sub>2</sub> has poor rate performance. Exactly, the discharge capacities of MoS<sub>2</sub>@NC composites at 10th, 20th, 30th, 40th, and 50th are 484, 456, 425, 408 and 393 mAh g<sup>-1</sup>, respectively, while for pure MoS<sub>2</sub>, the discharge capacity at 2.0 A g<sup>-1</sup> (50th) is only 254 mAh g<sup>-1</sup>. The poor rate performance of pure MoS<sub>2</sub> is caused by excessive volume expansion during cycling. Meanwhile, it also confirmed that carbon-coated can improve the electrochemical stability of MoS<sub>2</sub>. From Fig. 7b, stable cycling stability of MoS<sub>2</sub>@NC anodes which 481 mAh g<sup>-1</sup>

can be kept after 100 cycles at a current density of 0.1 A g<sup>-1</sup> is better than pure MoS<sub>2</sub> anodes. The retention capacity of MoS<sub>2</sub>@NC up to 70% is due to the carbon coating limiting the volume expansion of MoS<sub>2</sub> and maintaining its structural integrity. In addition, as shown in Fig. 7c, d, we also test the cycling performance of the MoS<sub>2</sub>@NC anode at current densities of 0.5 A g<sup>-1</sup> and 1 A g<sup>-1</sup> with high discharge specific capacities of 438 mAh g<sup>-1</sup> and 418 mAh g<sup>-1</sup> after 100 cycles. It can be observed that the prepared MoS<sub>2</sub>@NC composites exhibit enhanced electrochemical performance, and their preparation methods are simple and easy to operate.

The electrochemical impedance test is used to study the dynamics of electrode materials during charge and discharge process. Figure 8 is the Nyquist diagram of pure MoS<sub>2</sub> and MoS<sub>2</sub>@NC composite materials. They are tested after cycling 50 times at a current density of 500 mA used MoS<sub>2</sub> and MoS<sub>2</sub>@NC as sodium anode materials. The semicircle of

**Fig. 6** **a, b** The CV curves at  $0.1 \text{ mV s}^{-1}$  and Charge-discharge curves at  $0.1 \text{ A g}^{-1}$  of pure  $\text{MoS}_2$  for SIBs. **c, d** The CV curves at  $0.1 \text{ mV s}^{-1}$  and charge-discharge curves at  $0.1 \text{ A g}^{-1}$  of  $\text{MoS}_2@\text{NC}$  composites for SIBs

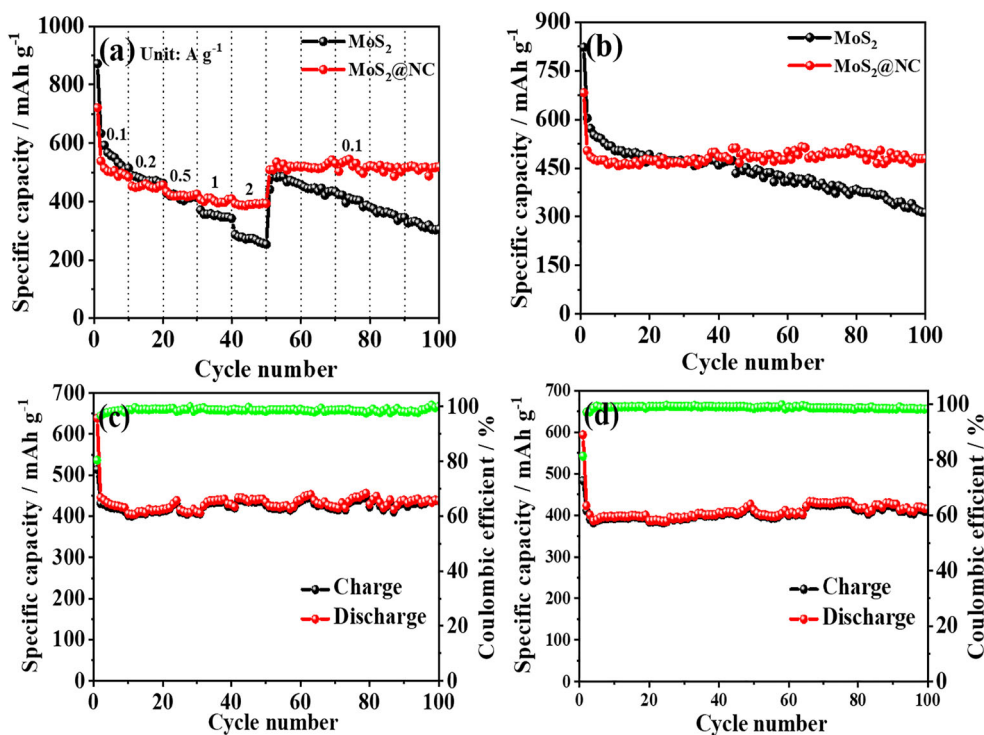


the intermediate frequency region diameter represents the size of the charge transfer resistance. As shown in Fig. 8, the charge transfer resistance of the  $\text{MoS}_2@\text{NC}$  composite ( $105 \text{ Ohm}$ ) is evidently lower than  $\text{MoS}_2$  ( $235 \text{ Ohm}$ ). The most

important reason is that the incorporation of carbon improves the conductivity of the composite.

The cyclic voltammetry-based analysis method is used to further study the electrochemical performance of  $\text{MoS}_2@\text{NC}$

**Fig. 7** **a** Rate performance and **b** cycling performance at  $0.1 \text{ A g}^{-1}$  of  $\text{MoS}_2@\text{NC}$  composites and pure  $\text{MoS}_2$ . **c, d** Cycling performance at  $0.5 \text{ A g}^{-1}$  (c) and  $1 \text{ A g}^{-1}$  (d) of  $\text{MoS}_2@\text{NC}$



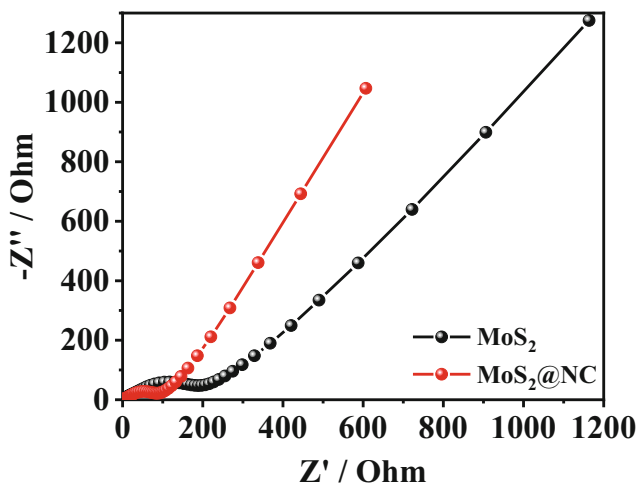


Fig. 8 Nyquist diagram of the MoS<sub>2</sub>@NC composites and pure MoS<sub>2</sub>

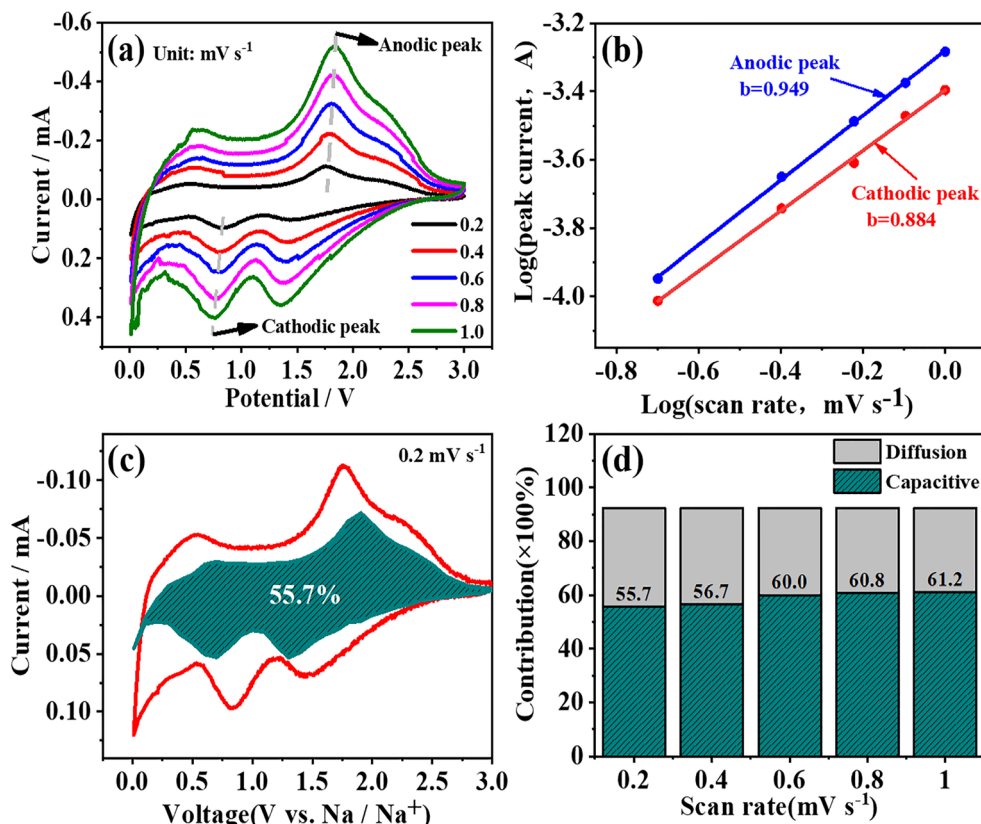
composites and to explain the contribution of diffusion control and surface capacitance control during the electrochemical reaction. Figure 9 a shows the CV curves of MoS<sub>2</sub>@NC composites measured at 0.2-, 0.4-, 0.6-, 0.8-, and 1.0- $\text{mV s}^{-1}$  scanning speeds. The five CV curves display the same shape and position of the cathode and anode peaks. The influence of capacitance on electrode material performance can be qualitatively analyzed by the relationship between  $i$  (current) and  $\nu$  (scan rate) of the CV curve  $i = a\nu^b$ , where  $a$  and  $b$  are both variable parameters. In addition, the value of  $b$  is derived from

the slope of  $\log(i)$  and  $\log(\nu)$  and the value of  $b$  is between 0.5 and 1. When the value of  $b$  is closer to 1, it means that the capacitance behavior contributes more. On the contrary, if the value of  $b$  is close to 0.5, it illustrates that the diffusion behavior is dominant. As seen in Fig. 9b, the  $b$  values of cathode peak and anode peak of MoS<sub>2</sub>@NC electrode materials are 0.95 and 0.88, respectively, which proves that the reaction process is controlled by both diffusion control and surface capacitance reaction, in which the capacitive behavior is dominant [36–38]. For a deeper quantitative analysis of the proportion of sodium-ion capacitance contribution at different scan rates, we implement the necessary calculations. Figure 9 d shows the sweep speeds of 0.2, 0.4, 0.6, 0.8, and 1.0  $\text{mV s}^{-1}$ . Its capacitance contribution ratios are 55.7%, 56.7%, 60.0%, 60.8%, and 61.2%.

### Conclusion

All in all, we have prepared MoS<sub>2</sub>@NC composites using dopamine as a nitrogen-containing carbon source and studied their electrochemical sodium storage capacity as SIBs anode material. Because the surface of MoS<sub>2</sub> was covered with a carbon coating, the volume expansion of MoS<sub>2</sub> was effectively suppressed, and its cycle performance and rate performance are greatly improved. Owing to these unique structures, after

Fig. 9 a CV curves of MoS<sub>2</sub>@NC composites at different scan rates of 0.2, 0.4, 0.6, 0.8 and 1.0  $\text{mV s}^{-1}$ . b Determination of the  $b$ -value using the relationship between peak current to sweep rate. c CV curves of MoS<sub>2</sub>@NC composites with separation between total current (solid line) and capacitive currents (shaded regions) at 0.2  $\text{mV s}^{-1}$ . d Separation of contributions from capacitive and diffusion-controlled capacities at different sweep rates



cycling 100 times at a current density of  $0.1 \text{ A g}^{-1}$ ,  $\text{MoS}_2/\text{NC}$  composites exhibited a reversible capacity of  $480 \text{ mAh g}^{-1}$  and showed excellent rate performance (at current densities of 0.1, 0.2, 0.5, 1 and  $2 \text{ A g}^{-1}$ , the corresponding capacities are 484, 456, 425, 408, and  $393 \text{ mAh g}^{-1}$ ). Therefore, our work provides a good idea for improving the electrochemistry of  $\text{MoS}_2$  as the anode material of SIBs.

**Funding information** This work was supported by the Science and Technology Program of Beijing Municipal Education Commission (SQKM201710005007).

## References

1. Yabuuchi N, Kubota K, Dahbi M, Komaba S (2014) Research development on sodium-ion batteries. *Chem Rev* 114(23):11636–11682. <https://doi.org/10.1021/cr500192f>
2. Ong SP, Chevrier VL, Hautier G, Jain A, Moore C, Kim S, Ma X, Ceder G (2011) Voltage, stability and diffusion barrier differences between sodium-ion and lithium-ion intercalation materials. *Energy Environ Sci* 4(9):3680. <https://doi.org/10.1039/c1ee01782a>
3. Hou H, Qiu X, Wei W, Zhang Y, Ji X (2017) Carbon anode materials for advanced sodium-ion batteries. *Adv Energy Mater* 7(24). <https://doi.org/10.1002/aenm.201602898>
4. Lao M, Zhang Y, Luo W, Yan Q, Sun W, Dou SX (2017) Alloy-based anode materials toward advanced sodium-ion batteries. *Adv Mater* 29(48). <https://doi.org/10.1002/adma.201700622>
5. Sun N, Guan Z, Liu Y, Cao Y, Zhu Q, Liu H, Wang Z, Zhang P, Xu B (2019) Extended “adsorption–insertion” model: a new insight into the sodium storage mechanism of hard carbons. *Adv Energy Mater* 9(32):1901351. <https://doi.org/10.1002/aenm.201901351>
6. Zhang X, Liu X, Yang C, Li N, Ji T, Yan K, Zhu B, Yin J, Zhao J, Li Y (2019) A  $\text{V}_2\text{O}_5$ -nanosheets-coated hard carbon fiber fabric as high-performance anode for sodium ion battery. *Surf Coat Technol* 358:661–666. <https://doi.org/10.1016/j.surfcoat.2018.11.096>
7. Zhang R, Li H, Sun D, Luan J, Huang X, Tang Y, Wang H (2018) Facile preparation of robust porous  $\text{MoS}_2/\text{C}$  nanosheet networks as anode material for sodium ion batteries. *J Mater Sci* 54(3):2472–2482. <https://doi.org/10.1007/s10853-018-2991-z>
8. Hou M, Qiu Y, Yan G, Wang J, Zhan D, Liu X, Gao J, Lai L (2019) Aging mechanism of  $\text{MoS}_2$  nanosheets confined in N-doped mesoporous carbon spheres for sodium-ion batteries. *Nano Energy* 62: 299–309. <https://doi.org/10.1016/j.nanoen.2019.05.048>
9. Sun Q, Dai Y, Ma Y, Jing T, Wei W, Huang B (2016) Ab initio prediction and characterization of  $\text{Mo}_2\text{C}$  monolayer as anodes for Lithium-ion and sodium-ion batteries. *J Phys Chem Lett* 7(6):937–943. <https://doi.org/10.1021/acs.jpcclett.6b00171>
10. Peng S, Han X, Li L, Zhu Z, Cheng F, Srinivansan M, Adams S, Ramakrishna S (2016) Unique cobalt sulfide/reduced graphene oxide composite as an anode for sodium-ion batteries with superior rate capability and long cycling stability. *Small* 12(10):1359–1368. <https://doi.org/10.1002/sml.201502788>
11. Xu X, Fan Z, Yu X, Ding S, Yu D, Lou XWD (2014) A nanosheets-on-channel architecture constructed from  $\text{MoS}_2$  and CMK-3 for high-capacity and long-cycle-life lithium storage. *Adv Energy Mater* 4(17). <https://doi.org/10.1002/aenm.201400902>
12. Gong F, Peng L, Liu M, Meng E, Li F (2019) Effect of RGO coating on lithium storage performance of monodispersed core-shell  $\text{MoS}_2$  superspheres. *J Mater Sci* 54(13):9643–9655. <https://doi.org/10.1007/s10853-019-03587-5>
13. Xiong QQ, Ji ZG (2016) Controllable growth of  $\text{MoS}_2/\text{C}$  flower-like microspheres with enhanced electrochemical performance for lithium ion batteries. *J Alloys Compd* 673:215–219. <https://doi.org/10.1016/j.jallcom.2016.02.253>
14. Liu Y, Zhao Y, Jiao L, Chen J (2014) A graphene-like  $\text{MoS}_2$ /graphene nanocomposite as a high performance anode for lithium ion batteries. *J Mater Chem A* 2(32):13109–13115. <https://doi.org/10.1039/c4ta01644k>
15. Hu S, Chen W, Zhou J, Yin F, Uchaker E, Zhang Q, Cao G (2014) Preparation of carbon coated  $\text{MoS}_2$  flower-like nanostructure with self-assembled nanosheets as high-performance lithium-ion battery anodes. *J Mater Chem A* 2(21):7862. <https://doi.org/10.1039/c4ta01247j>
16. Sun P, Zhang W, Hu X, Yuan L, Huang Y (2014) Synthesis of hierarchical  $\text{MoS}_2$  and its electrochemical performance as an anode material for lithium-ion batteries. *J Mater Chem A* 2(10):3498–3504. <https://doi.org/10.1039/c3ta13994h>
17. Yang T, Chen Y, Qu B, Mei L, Lei D, Zhang H, Li Q, Wang T (2014) Construction of 3D flower-like  $\text{MoS}_2$  spheres with nanosheets as anode materials for high-performance lithium ion batteries. *Electrochim Acta* 115:165–169. <https://doi.org/10.1016/j.electacta.2013.10.098>
18. Yuan G, Wang G, Wang H, Bai J (2016) Half-cell and full-cell investigations of 3D hierarchical  $\text{MoS}_2$ /graphene composite on anode performance in lithium-ion batteries. *J Alloys Compd* 660:62–72. <https://doi.org/10.1016/j.jallcom.2015.11.079>
19. Li Y, Mao H, Zheng C, Wang J, Che Z, Wei M (2020) Compositing reduced graphene oxide with interlayer spacing enlarged  $\text{MoS}_2$  for performance enhanced sodium-ion batteries. *J Phys Chem Solids*: 136. <https://doi.org/10.1016/j.jpcc.2019.109163>
20. Chen F, Wu L, Zhou Z, Ju J, Zhao Z, Zhong M, Kuang T (2019)  $\text{MoS}_2$  decorated lignin-derived hierarchical mesoporous carbon hybrid nanospheres with exceptional Li-ion battery cycle stability. *Chin Chem Lett* 30(1):197–202. <https://doi.org/10.1016/j.ccl.2018.10.007>
21. Feng M, Zhang M, Zhang H, Liu X, Feng H (2019) Room-temperature carbon coating on  $\text{MoS}_2$ /Graphene hybrids with carbon dioxide for enhanced sodium storage. *Carbon* 153:217–224. <https://doi.org/10.1016/j.carbon.2019.07.021>
22. Li N, Liu Z, Gao Q, Li X, Wang R, Yan X, Li Y (2017) In situ synthesis of concentric C@ $\text{MoS}_2$  core-shell nanospheres as anode for lithium ion battery. *J Mater Sci* 52(22):13183–13191. <https://doi.org/10.1007/s10853-017-1411-0>
23. Wang Y, Jin Y, Li S, Han J, Ju Z, Jia M (2018) Flower-like  $\text{MoS}_2$  supported on three-dimensional graphene aerogels as high-performance anode materials for sodium-ion batteries. *Ionics* 24(11):3431–3437. <https://doi.org/10.1007/s11581-018-2528-0>
24. Cheng A, Zhang H, Zhong W, Li Z, Tang Y, Li Z (2019) Enhanced electrochemical properties of single-layer  $\text{MoS}_2$  embedded in carbon nanofibers by electrospinning as anode materials for sodium-ion batteries. *J Electroanal Chem* 843:31–36. <https://doi.org/10.1016/j.jelechem.2019.04.059>
25. Lin M, Deng M, Zhou C, Shu Y, Yang L, Ouyang L, Gao Q, Zhu M (2019) Popcorn derived carbon enhances the cyclic stability of  $\text{MoS}_2$  as an anode material for sodium-ion batteries. *Electrochim Acta* 309:25–33. <https://doi.org/10.1016/j.electacta.2019.04.070>
26. Wang S, Cao F, Li Y, Zhang Z, Zhou D, Yang Y, Tang Z (2019)  $\text{MoS}_2$ -coupled carbon nanosheets encapsulated on sodium titanate nanowires as super-durable anode material for sodium-ion batteries. *Adv Sci (Weinh)* 6(10):1900028. <https://doi.org/10.1002/adv.201900028>
27. Hu Y-Y, Bai Y-L, Wu X-Y, Wei X, Wang K-X, Chen J-S (2019)  $\text{MoS}_2$  nanoflakes integrated in a 3D carbon framework for high-performance sodium-ion batteries. *J Alloys Compd* 797:1126–1132. <https://doi.org/10.1016/j.jallcom.2019.05.142>
28. Pan E, Jin Y, Zhao C, Jia M, Chang Q, Zhang R, Jia M (2019) Mesoporous  $\text{Sn}_4\text{P}_3$ -graphene aerogel composite as a high-



- performance anode in sodium ion batteries. *Appl Surf Sci* 475:12–19. <https://doi.org/10.1016/j.apsusc.2018.12.259>
29. Jia M, Jin Y, Zhao P, Zhao C, Jia M, Wang L, He X (2019) Hollow NiCoSe<sub>2</sub> microspheres@N-doped carbon as high-performance pseudocapacitive anode materials for sodium ion batteries. *Electrochim Acta* 310:230–239. <https://doi.org/10.1016/j.electacta.2019.04.124>
30. Han L, Wu S, Hu Z, Chen M, Ding J, Wang S (2020) Hierarchically porous MoS<sub>2</sub>-carbon hollow rhomboids for superior performance of the anode of sodium-ion batteries. *ACS Appl Mater Interfaces* 12(9):10402–10409. <https://doi.org/10.1021/acsami.9b21365>
31. Zhang R, Wang J, Li C, Liu T, Yao T, Zhu L, Han X, Wang H (2020) Facile synthesis of hybrid MoS<sub>2</sub>/graphene nanosheets as high-performance anode for sodium-ion batteries. *Ionics* 26:711–717. <https://doi.org/10.1007/s11581-019-03235-7>
32. Wang S, Tu J, Yuan Y, Ma R, Jiao S (2016) Sodium modified molybdenum sulfide via molten salt electrolysis as an anode material for high performance sodium-ion batteries. *Phys Chem Chem Phys* 8:3204
33. Anwer S, Huang Y, Li B, Govindan B, Liao K, Cantwell WJ, Wu F, Chen R, Zheng L (2019) Nature-inspired, graphene-wrapped 3D MoS<sub>2</sub> ultrathin microflower architecture as a high-performance anode material for sodium-ion batteries. *ACS Appl Mater Interfaces* 11(25):22323–22331. <https://doi.org/10.1021/acsami.9b04260>
34. Brown E, Yan P, Tekik H, Elangovan A, Wang J, Lin D, Li J (2019) 3D printing of hybrid MoS<sub>2</sub>-graphene aerogels as highly porous electrode materials for sodium ion battery anodes. *Mater Des* 170:107689. <https://doi.org/10.1016/j.matdes.2019.107689>
35. Wang C, Zhan C, Ren X, Lv R, Shen W, Kang F, Huang Z-H (2019) MoS<sub>2</sub>/carbon composites prepared by ball-milling and pyrolysis for the high-rate and stable anode of lithium ion capacitors. *RSC Adv* 9(72):42316–42323. <https://doi.org/10.1039/c9ra09411c>
36. Zou J, Li F, Bissett MA, Kim F, Hardwick LJ (2020) Intercalation behaviour of Li and Na into 3-layer and multilayer MoS<sub>2</sub> flakes. *Electrochim Acta* 331:135284. <https://doi.org/10.1016/j.electacta.2019.135284>
37. Wang J, Han L, Li X, Zeng L, Wei M (2019) MoS<sub>2</sub> hollow spheres in ether-based electrolyte for high performance sodium ion battery. *J Colloid Interface Sci* 548:20–24. <https://doi.org/10.1016/j.jcis.2019.04.025>
38. Zeng L, Luo F, Chen X, Xu L, Xiong P, Feng X, Luo Y, Chen Q, Wei M, Qian Q (2019) An ultra-small few-layer MoS<sub>2</sub>-hierarchical porous carbon fiber composite obtained via nanocasting synthesis for sodium-ion battery anodes with excellent long-term cycling performance. *Dalton Trans* 48(13):4149–4156. <https://doi.org/10.1039/c8dt04744h>

**Publisher's note** Springer Nature remains neutral with regard to jurisdictional claims in published maps and institutional affiliations.